Flexible and High Thermal Conductivity Composites Based on Graphite Nanoplates Paper Impregnated with Polydimethylsiloxane

Journal of
Composites Science

MDPI

Article

Flexible and High Thermal Conductivity Composites Based on Graphite Nanoplates Paper Impregnated with Polydimethylsiloxane

Daniele Battegazzore, Erica Fadda and Alberto Fina *

Dipartimento di Scienza Applicata e Tecnologia, Politecnico di Torino, Alessandria Campus, Viale Teresa Michel 5, 15121 Alessandria, Italy; daniele.battegazzore@polito.it (D.B.); ericafadda@virgilio.it (E.F.)
* Correspondence: alberto.fina@polito.it

Abstract: This paper deals with the design, preparation, and characterization of conductive and flexible nanopapers based on graphite nanoplates (GNP) and polydimethylsiloxane (PDMS). Highly porous GNP nanopapers were first prepared by filtration from a GNP suspension in a solvent. Subsequently, PDMS impregnation was carried out to obtain a composite material. By varying the concentration of the polymer solution and the deposition time, PDMS/GNP nanopapers were produced with a wide range of PDMS contents, porosities, and densities. Thermal diffusivity of the composite films (both in-plane and cross-plane) were measured and correlated with the structure of the nanopapers. Selected formulations were investigated in detail for their physical, thermal, and mechanical properties, exhibiting high flexibility and resistance to more than 50 repeated bendings, stiffness of up to 1.3 MPa, and thermal conductivity of up to 25 W/m·K. Based on the properties obtained, the materials presented in this paper may find applications in modern lightweight and flexible electronic devices.

Keywords: graphite nanoplates; nanopapers; thermal conductivity; graphite nanoplates polymer composite

Citation: Battegazzore, D.; Fadda, E.; Fina, A. Flexible and High Thermal Conductivity Composites Based on Graphite Nanoplates Paper Impregnated with Polydimethylsiloxane. *J. Compos. Sci.* **2021**, *5*, 309. https://doi.org/10.3390/jcs5120309

Academic Editors: Marco Monti and Ilaria Armentano

Received: 9 November 2021
Accepted: 21 November 2021
Published: 25 November 2021

1. Introduction

Research on materials and nanotechnologies has paid a lot of attention to graphene for its peculiar properties, such as electrical and thermal conductivity, mechanical properties, and large specific area, which make it a potential candidate in several applications [1–3]. The term graphene refers to a carbon sheet with a hexagonal structure sp^2 hybridized, with the thickness of a single atom. The availability of this material for bulk applications remains very limited, while several graphene-related materials are now widely available, including graphene oxide, reduced graphene oxide, multilayered graphene, and graphite nanoplates (GNPs) [4]. In particular, GNPs have been widely used in composite materials, thanks to their good compromise between properties, availability, and cost. Currently, a wide research interest is focused on the manufacture of composites with high thermal conductivity properties [5–8]. Enhanced thermal conductivity has been obtained for various polymer matrices; however, the observed improvement is limited by difficulties in the dispersion of conductive particles and the high interfacial thermal resistance between conductive particles and the matrix [9,10]. Furthermore, it has been demonstrated that a higher concentration of microstructural defects reduces the thermal conductivity of graphene and related materials [11,12]. Inevitably, this is also directly reflected in the thermal conductivity of the relative polymer nanocomposites, where low-quality graphene or graphene-related materials do not allow achieving satisfactory performance [5,13].

Among the many different polymers used to prepare thermally conductive polymer nanocomposites, polydimethylsiloxane (PDMS) is an almost unique material, coupling ease of processing into a cross-linked structure with high flexibility and elongation prop-

erties, as well as remarkable chemical resistance. These properties are highly desirable in flexible heat exchanger materials, which justifies the interest in PDMS as a polymer matrix for thermally conductive composites [14] and nanocomposites. As for the latter, Kong et al. [15] investigated PDMS composites based on exfoliated graphite nanoplates, in which a 4 wt.% filler content yielded a thermal conductivity of 0.36 W/m·K and a 2.5 MPa tensile strength. Zhao et al. [16] reported a two-fold increase in the thermal conductivity of multilayer graphene flakes/PDMS composite (0.40 W/m·K) with respect to the neat PDMS when adding 2.7 vol.% of conductive particles. In the same paper, conductivity was further increased to 1.08 W/m·K, thanks to the combined use of an interconnected network of graphene foam and multilayer graphene flakes. In terms of mechanical properties, the same material exhibited a 4 MPa modulus, 1.7 MPa strength, and 60% elongation for the best thermally conductive sample. Similar results were reported by Zhang et al. [17], with a thermal conductivity of 0.58 W/m·K for the 1 wt.% graphene aerogel (GA)/PDMS composite fabricated by impregnating 3D GA frameworks with PDMS and a vacuum curing process. Tao et al. [18] reported dispersion of expanded graphite (EG) in polydimethylsiloxane (PDMS) in a hexane solution, followed by hot pressing at 80 °C, leading to a 4.70 W/m·K thermal conductivity at 10 wt.% EG. Flexible graphene-based composites were fabricated using a casting method by Oliva et al. [19]. A graphene solution was poured in a plastic mould, and the solvent was evaporated. Afterwards, an acrylic solution with a photoinitiator was dropped on the dry graphene and cured with UV light. In this way, highly GNP-loaded nanocomposites were prepared, yielding thermal conductivity values of 11.70 W/m·K, 7.76 W/m·K, and 3.74 W/m·K for the through-plane direction with 75, 50, and 25 wt.% of GNP, respectively [19]. Besides, the presence of GNP was also reported to strongly affect the mechanical properties of composites, with an elastic modulus of 67.7 MPa and an ultimate tensile strength of 3.34 MPa for the formulation containing 25 wt.% GNP. Han et al. [20] reported a procedure to produce highly oriented PDMS/graphene composites based on the winding of few layer graphene foils and subsequent impregnation with PDMS. After curing and sectioning, composite slices were obtained with vertically aligned graphene, exhibiting a conductivity of 2.18 W/m·K with 16.6 wt.% graphene nanosheets. Fang et al. [21,22] reported the impregnation of PDMS into a preformed porous structure obtained by the deposition of graphene onto a nickel foam, which was then dissolved prior to PDMS impregnation. In this way, a material with a continuous network of graphene yielding a thermal conductivity of 22 W/m·K was obtained.

Targeting high-end thermal conductivity, production of nanopapers by self-assembly during filtration of conductive particles in a solvent was also widely studied. Depending on their geometrical features, the strength of interaction between particles, and preparation conditions, these may produce different structural organizations, from tightly packed to highly porous films. Graphene and related materials, including multilayer graphene, reduced graphene oxide and graphite nanoplates, and currently represent the most interesting materials to prepare thermally conductive nanopapers [23–26]. The main limitation in the performance of these nanopapers is in their limited toughness and deformability, which reflects the weak interactions between nanoparticles [27–30]. To enhance thermal and mechanical properties, both small molecules and macromolecules have been proposed. Bispyrene molecules have indeed been found to drive self-assembly of GNP and improve contacts between those, eventually enhancing the thermal conductivity of nanopapers [31]. The inclusion of macromolecules into the nanopapers has also been explored to enhance their toughness and deformability [32–34], but the amount of polymer and its crystalline organization [35] should be carefully controlled to avoid a dramatic decrease in the thermal conductivity of the nanostructure.

Building on the previous state of the art, this paper focused on the preparation and characterization of highly conductive and flexible sheets by PDMS impregnation into GNP-based nanopapers. In particular, by varying the concentration of the PDMS solution and the deposition steps, a range of different densities and thermal conductivities was obtained, delivering a set of materials for possible applications in heat spreader devices.

2. Materials and Methods

2.1. Materials

The GNP used in this work was kindly supplied by Avanzare (Navarrete, La Rioja, Spain) and prepared via rapid thermal expansion of overoxidized intercalated graphite, as previously reported [36], and used as supplied without any further treatments. This GNP grade is constituted by low structural defectiveness and well-separated large (tens of μm) wavy thin layers. A detailed characterization of this GNP grade was previously reported [5] (therein referred to as GRM-2). Dimethylformamide (DMF, 99.8%) and hexane (>95%) were purchased from Sigma-Aldrich.

2.2. Nanopaper Production

A suspension containing 25 mg of GNP and 75 mL of DMF was prepared inside a 250 mL glass beaker and sonicated with an immersion tip (Sonics Vibracell VC505, Sonics & Materials Inc. (Newtown, CT, USA), using a 13 mm diameter Ti-alloy tip, a time of 15 min, a pulse of 30 s ON and 30 s OFF, a power of 500 W, an amplitude of 30%). The suspension was then removed from the sonicator, and after about 30 min of cooling, it was poured onto a polyamide filtering membrane with a 47 mm diameter and a porosity of 0.45 μm and slowly filtered with the help of a vacuum pump (10–15 min). First, the filtered film was covered with 30 mL of ethanol and then with 30 mL of diethyl ether, vacuuming each of the two solvents to eliminate them and finally leaving the pump attached for 10 min to ensure that the sheet was dry. Then, the GNP supported onto the membrane was dried in a vacuum oven at 70 °C for at least 2 h in order to eliminate the remaining solvents and carefully detached to obtain self-standing nanopapers. GNP nanopapers were placed on a Teflon surface and impregnated with PDMS (Sylgard® 184 by Dow) in hexane, with variable concentrations, namely, 9% (1:10), 17% (1:5), and 29% wt. (1:2.5). A cross-linker (Sylgard® 184 Curing Agent by Dow) was also added in the solution at 10% with respect to PDMS. A volume of 0.5 mL for each impregnation step was homogeneously dripped manually on the film surface using a pipette and let dry in the hood at room temperature for 30 min. Finally, the sample was placed in an oven at 70 °C for 24 h for cross-linking. After this time, the composite was carefully detached from the Teflon support. The samples were coded in the form *c% nx*, where *c* is the concentration (wt.%) of the solutions and *n* is the number of impregnation steps. Larger nanopapers (90 mm diameter, referred to as L, following the above defined materials coding) were also prepared, scaling up the suspension to 108 mg GNP in 327 mL DMF. To prevent excessive heating and evaporation of DMF during sonication, a larger beaker was used, placing it in a water bath at a temperature of about 5 °C with different operating conditions (time, 20 min; pulse, 15 s ON and 30 s OFF; power, 500 W; amplitude 30%). Selected nanopapers underwent compression during the polymer cross-linking (referred to as P, following the above defined materials coding), under a pressure of 2.2 MPa for 2 h at a temperature of 70 °C, using a manual hydraulic press (Specac) between two Teflon plates as supports. In pressed nanopapers, the cross-linking phase was completed in an oven for 16 h at 70 °C.

2.3. Characterization Methods

To calculate the densities, nanopapers were die-cut into 25 mm diameter disks, and the method of weighing the disks in air and in water according to the ASTM D792, ISO 1183 standard, was performed. The density found is the one defined as ρ_{sample} in the text.

The volume percentage of voids in the sample was calculated by the formula:

$$\text{Porosity (vol.\%)} = \left(1 - \left(\frac{\rho_{\text{sample}}}{\left(\frac{P_{GNP}}{P_{\text{impregnated}}}\right)\cdot \rho_{GNP} + \left(1 - \frac{P_{GNP}}{P_{\text{impregnated}}}\right)\cdot \rho_{PDMS}}\right)\right)\cdot 100$$

where $\rho_{GNP} = 2.267$ g/cm^3 and $\rho_{PDMS} = 0.958$ g/cm^3, and P_{GNP} and $P_{impregnated}$ are the nanopaper weights before and after impregnation. The same weights (P_{GNP} and $P_{impregnated}$) were used to evaluate the wt.% of GNP present in the composite.

$$\text{wt.\% GNP} = \left[1 - \frac{\left(P_{impregnated} - P_{GNP}\right)}{P_{impregnated}}\right] * 100$$

$$\text{GNP(vol.\%)} = (100 - \text{porosity}) * \left(\frac{\frac{\text{wt.\% GNP}}{\rho_{grafene}}}{\frac{\text{wt.\% GNP}}{\rho_{grafene}} - (100 - \text{wt.\% GNP}) * \rho_{PDMS}}\right)$$

$$\text{PDMS(vol.\%)} = 100 - \text{GNP(vol.\%)} - \text{Porosity(vol.\%)}$$

The thermal diffusivity (α) of the prepared nanopapers was measured at 25 °C using a Netzsch LFA 467 HyperFlash® xenon light flash analysis (LFA) on the same 25 mm disk used to calculate density. The nanopapers were measured for both cross-plane and in-plane diffusivity. Measurements were carried out with consistent flash parameters (230 V, 200 µs) and repeated five times for each specimen to get average thermal diffusivity and standard deviation.

Thermal conductivity was calculated from the measured diffusivity values, multiplied by the density and specific heat capacity of the different materials. The value of the specific heat capacity for impregnated nanopapers was calculated as a weighted average with respect to the wt.% of GNP and PDMS in the sample

$$C_{p\ sample} = C_{p\ GNP} \cdot \frac{\text{wt.\% GNP}}{100} + C_{p\ PDMS} \cdot \frac{(100 - \text{wt.\% GNP})}{100}$$

with $C_{p\ GNP} = 0.71$ kJ/kg·K; $C_{p\ PDMS} = 1.46$ kJ/kg·K.

Tensile tests were conducted using the dynamometer Instron Model 5966 equipped with a 50 N load cell. The pneumatic clamps chosen were equipped with flat 25 × 25 mm^2 smooth faces. The gauge length was set at 20 mm and a preload force at 0.02 N to ensure the sample straightness at the start of the test. A crosshead speed of 0.1 mm/min was established, and the end of the test was considered when the force was below the value of 0.1 N. The tests provided data on the elastic modulus (E), the maximum stress (σ_{max}), and the elongation at maximum stress ($\varepsilon_{max\ stress}$) of the samples. The samples for the mechanical properties were obtained by cutting specimens of 10 × 40 mm^2 size, and three samples were tested for each formulation to get average values and their standard deviation.

Morphological characterization of both nanopapers and nanocomposites was performed by a high-resolution field emission scanning electron microscope (FESEM, Merlin 4248 by Zeiss) operated at 3 kV or a scanning electron microscope (SEM, EVO 15 by Zeiss) at a beam voltage of 20 kV and a working distance of 8.5 mm. A nanopaper and composites were cryofractured in liquid nitrogen and directly observed without further preparation.

A qualitative bending test was carried out on the nanopapers manually: using a tweezer, a 25 mm diameter specimen was held approximately in the middle of the sample, which was bent to 180° using a second tweezer. Immediately after, the sample was brought back to planar and bent in the same way but in the opposite direction. This operation series is referred to as one bending cycle.

3. Results and Discussion

3.1. Characterization of Pristine GNP Nanopapers

Pristine GNP nanopapers were observed by SEM and expectedly found to be highly porous (Figure 1a,c), with thickness in the range of 200–300 µm and density in the range of 0.07–0.12 mg/mm^3, which is perfectly suitable for solution impregnation with a polymer solution.

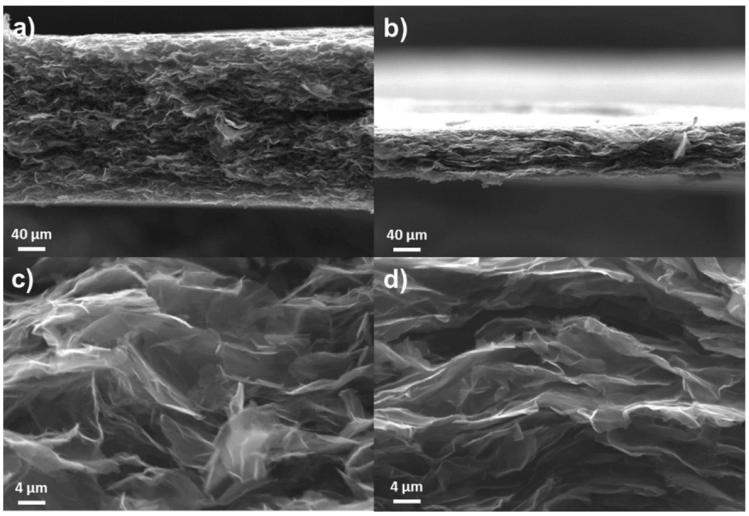

Figure 1. SEM micrographs of pristine GNP nanopaper: unpressed (**a**,**c**) and pressed (**b**,**d**). Dark areas in between flakes correspond to porosity of the nanopapers.

Uniaxial compression was applied to consolidate the structure and yielded a significant density increase, still associated with remarkable porosity in the range of 80% (Table 1), which was also confirmed by SEM imaging (Figure 1b,d). Indeed, a significant reduction in thickness from about 300 to 80 µm was observed upon compression of a GNP nanopaper, along with a qualitatively higher in-plane orientation of nanoflakes. The thermal conductivity of pristine GNP papers was calculated both as obtained from the filtration of GNP suspension and after compression (Table 1), to investigate changes upon compression, as a consequence of densification. Indeed, the better in-plane orientation of GNP plates increased the in-plane diffusivity, while the cross-plane diffusivity decreased. Thanks to the densification of the sample, the cross-plane conductivity turned out to be practically equal between the pristine and pressed samples, while in in-plane direction, it more than quadrupled (Table 1) to approximately 40 W/m·K. It is worth mentioning that this value is still relatively low compared with previously reported GNP nanopapers [26,31,37] owing to the relatively low density.

Table 1. Density, porosity, and thermal diffusivity and conductivity values for pristine GNP nanopapers.

Sample Code	Density ρ (g/cm^3)	Vol.% Porosity	Diffusivity α (mm^2/s)		Conductivity (W/m·K)	
			Cross-Plane	In-Plane	Cross-Plane	In-Plane
GNP	0.12 ± 0.01	95 ± 2	9.25 ± 0.06	101.2 ± 4.8	0.79 ± 0.07	8.6 ± 1.2
GNP-P	0.37 ± 0.02	83 ± 2	2.74 ± 0.03	152.3 ± 2.2	0.71 ± 0.06	39.5 ± 3.3

Besides the thermal conductivity performance, it has to be mentioned that pristine GNP nanopapers are intrinsically brittle, which limits their practical application as heat spreaders. To characterize this aspect, tensile tests were carried out on nanopapers. The uncompressed GNP nanopaper showed a very low modulus (ca. 31 MPa) and strength (ca. 0.1 MPa) (Table 2), suggesting that the contacts between GNP plates were rather weak as obtained after filtration, yielding a poor stress transfer within the structure. On the other hand, pressing strongly improved the mechanical properties, reaching a modulus of about 1 GPa and a maximum stress of 4 MPa, while the deformation at the maximum stress was practically independent on pressing (Table 2). It is worth mentioning that significant experimental deviations were found in both as obtained and pressed GNP nanopapers, likely due to the presence of microdefects, as a consequence of possible GNP agglomerates within the suspension and/or microcracks produced during nanopaper handling and specimen preparation, owing to their remarkable brittleness.

Table 2. Mechanical properties of pristine GNP nanopapers.

Sample	E (MPa)	σ_{max} (MPa)	$\varepsilon_{max\ stress}$ (%)
GNP	31.1 ± 3.1	0.13 ± 0.03	1.1 ± 0.2
GNP-P	1186 ± 343	4.3 ± 0.9	0.9 ± 0.2

3.2. Characterization of GNP Nanopapers Impregnated with PDMS

To consolidate the GNP structure in nanopapers and overcome the brittleness limitations, GNP papers were impregnated with PDMS. Indeed, the highly porous structure allows for an optimal absorption of PDMS solution and quick polymer deposition, thanks to the rapid evaporation of the solvent. Based on the preliminary impregnation tests on small samples reported in Supporting Information, selected formulations were further investigated, preparing larger (L) nanopapers, targeting GNP contents of ~50 wt.%, ~25% wt.%, and ~15% wt.%. To reach these PDMS fractions, both the concentration of the solution and the number of depositions were adjusted, eventually leading to PDMS wt.% close to the targets, as reported in Table 3, along with densities and thermal properties of the different polymer-impregnated nanopapers.

Table 3. Density, GNP content, porosity, and thermal diffusivity and conductivity values for PDMS/GNP L nanopapers.

Sample Code	Density ρ (g/cm^3)	wt.% GNP	Vol.% Porosity	Diffusivity α (mm^2/s)		Conductivity (W/m·K)	
				Cross-Plane	In-Plane	Cross-Plane	In-Plane
9% 1× L	0.11 ± 0.02	55.6 ± 0.1	93 ± 4	1.93 ± 0.01	44.5 ± 1.8	0.23 ± 0.03	5.4 ± 0.9
9% 3× L	0.28 ± 0.02	30.3 ± 0.1	79 ± 4	2.91 ± 0.01	34.4 ± 1.9	1.00 ± 0.08	11.9 ± 1.5
29% 2× L	0.60 ± 0.02	13.2 ± 0.1	47 ± 4	1.02 ± 0.01	7.8 ± 0.3	0.83 ± 0.04	6.4 ± 0.4
9% 3× L-P	0.91 ± 0.04	31.4 ± 0.6	27 ± 4	2.73 ± 0.01	22.8 ± 0.6	3.1 ± 0.1	25.6 ± 1.4

The heat conduction properties in cross-plane and in-plane for unpressed PDMS/GNP nanopapers are summarized in Figure 2, showing that the best performance is obtained with triple deposition of a 9% PDMS solution. Indeed, while diffusivity values are directly dependent on the GNP fraction, the increase in density obtained when progressively filling voids with PDMS is also affecting the thermal conductivity of the nanopaper, leading to the best performance for the intermediate GNP concentration.

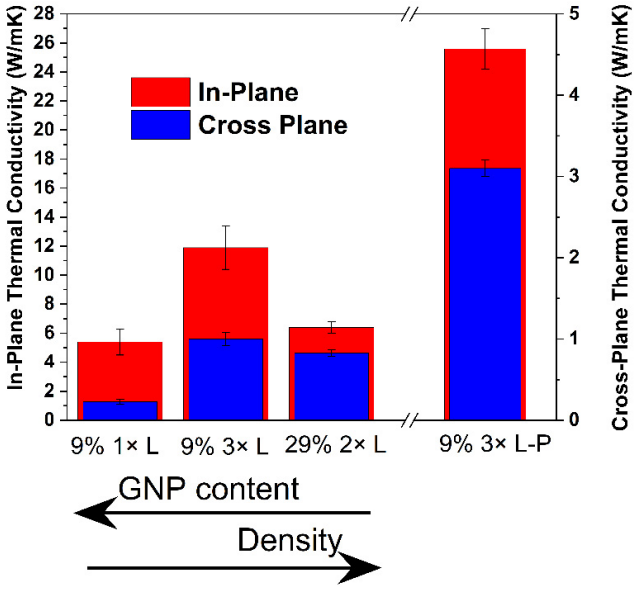

Figure 2. In-plane and cross-plane thermal conductivities for PDMS/GNP nanopapers.

To further enhance the nanopaper density, the 9% 3× L impregnated nanopaper underwent mechanical compression during cross-linking. The result of this compression generated a more compact nanopaper with a three-fold increase in the density (0.91 vs. 0.28 g/cm^3), leading to a dramatic enhancement in the in-plane thermal conductivity to ca. 25 W/m·K. The SEM micrograph comparison between standard vs. pressed nanopapers (Figure 3) confirmed the reduction in the thickness for the compressed PDMS/GNP nanopaper, as well as a denser structure, with more evident polymer flaps connecting the various GNP lamellae.

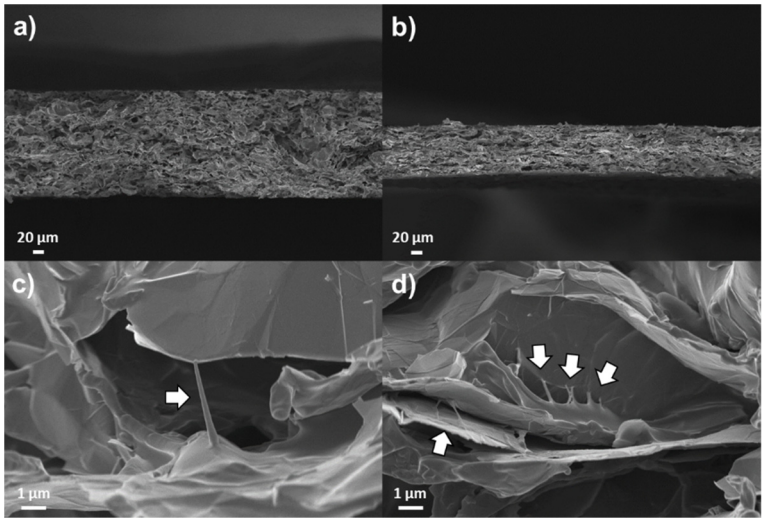

Figure 3. FESEM micrographs for PDMS/GNP nanopapers, 9% 3× L (**a**,**c**) and 9% 3× L-P (**b**,**d**), with highlighted polymer flaps. The dark areas in between flakes correspond to the porosity of the nanopapers.

Envisaging possible applications of PDMS/GNP nanopapers as a flexible heat spreader, the mechanical properties were investigated in tensile mode. The elastic modulus (E), the maximum stress (σ_{max}), and the elongation at maximum stress ($\varepsilon_{max\ stress}$) were evaluated and are reported in Table 4 and Figure 4, while representative stress–strain curves are reported in Figure S3.

Pristine GNP nanopapers exhibit limited mechanical performances, suggesting mechanical performance to be controlled by the weak interactions between graphite nanoplates. The addition of soft and deformable PDMS, acting as a binder in the GNP network, generally enhanced mechanical properties in all regards of stiffness, strength, and toughness. The best mechanical performances are confirmed for the 9% 3× L-P nanopaper formulation. Indeed, the best elastic modulus (148 ± 7 MPa) and maximum stress (1.34 ± 0.10 MPa) are obtained, which is about three times higher than unpressed samples, while the elongation at maximum stress is comparable to the best unpressed performance (2.3 ± 0.5%).

Table 4. Mechanical properties of GNP and PDMS/GNP nanopapers.

Sample	E (MPa)	σ_{max} (MPa)	$\varepsilon_{max\ stress}$ (%)
PDMS	1.7 ± 0.2	3.98 ± 0.40	135 ± 3
GNP	31.1 ± 3.1	0.13 ± 0.03	1.1 ± 0.2
9% 1× L	22.6 ± 1.6	0.17 ± 0.01	1.3 ± 0.2
9% 3× L	52.0 ± 13.9	0.45 ± 0.01	1.7 ± 0.3
29% 2× L	49.4 ± 7.9	0.44 ± 0.08	2.2 ± 0.5
9% 3× L-P	148 ± 7	1.34 ± 0.10	2.3 ± 0.5

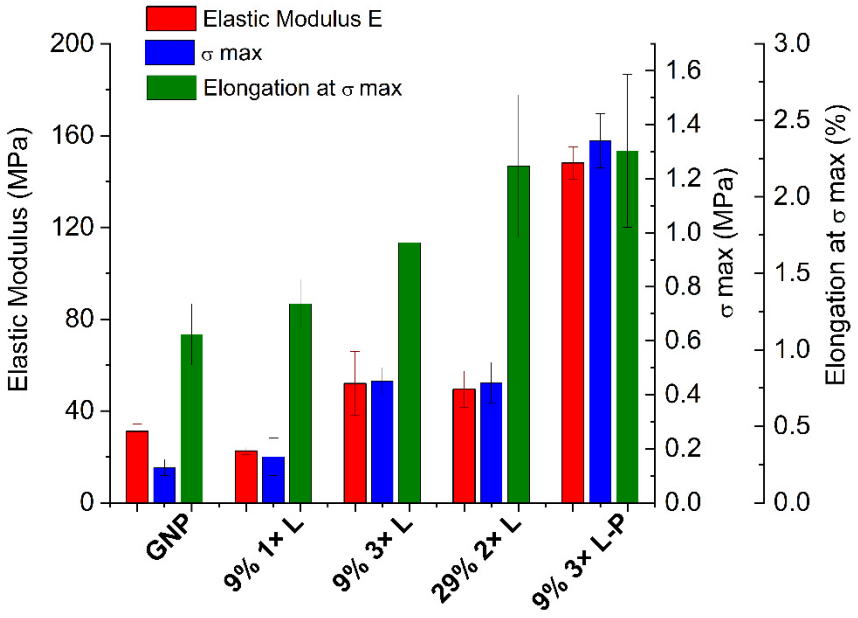

Figure 4. Mechanical properties of PDMS/GNP nanopapers.

Comparing the results of strength and conductivity for our materials with previously reported data on PDMS/GNP composites (Figure 5), it clearly appears that superior conductivity was obtained compared with previous literature. Furthermore, our best-performing nanopaper closely competes with the material proposed by Fang et al. [21], which is, however, produced by a more complex and energy-consuming procedure, requiring GNP deposition onto a metal foam, subsequently removed via acid treatment, before PDMS impregnation.

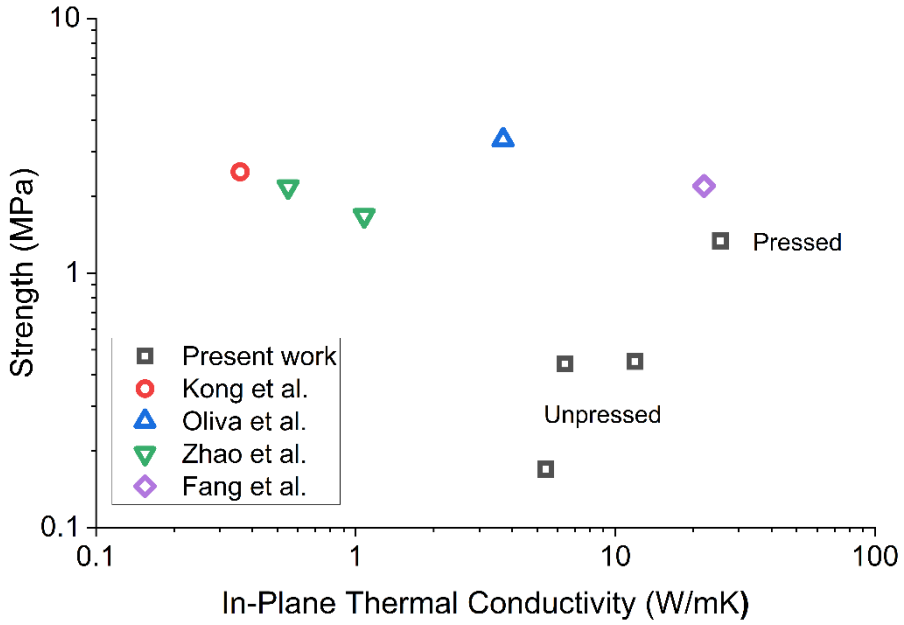

Figure 5. Combined strength and thermal conductivity plot of PDMS/GNP composites [15,16,19,21].

As a last practical evaluation to test the resistance to multiple deformations, a qualitative bending test was carried out. The unpressed GNP nanopaper breaks on the first bending attempt, evidencing for its remarkable brittleness. The pressed GNP paper allows bending without breaking, but nonrestorable cracks appear after 5 cycles (GNP-P in Figure 6), leading to the nanopaper breaking after approximately 10 cycles. Unpressed impregnated GNP papers also withstand only a few bending cycles, whereas an impreg-

nated and pressed sample does not undergo any visible damage variation even beyond 50 bending cycles (9% 3× L-P in Figure 6).

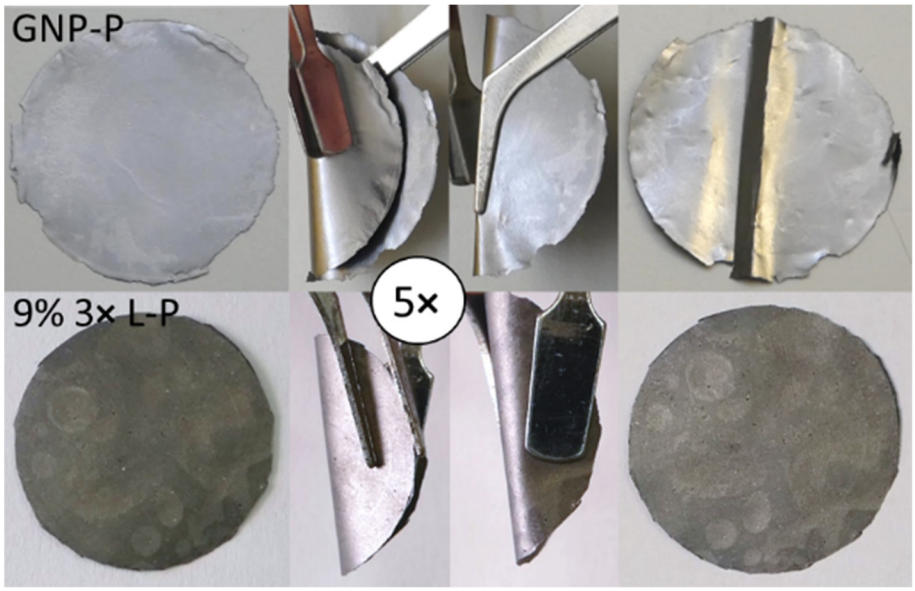

Figure 6. Test of resistance to multiple bending deformations of GNP-P and 9% 3× L-P samples. Images show the nanopapers before (**left**), during (**centre**), and after (**right**) bending.

4. Conclusions

The impregnation of PDMS within the porous structure of preformed nanopapers based on graphite nanoplates was successfully carried out by a simple casting method from a PDMS solution in hexane. The obtained PDMS/GNP nanopapers' porosity, obtained as an effect of the solvent evaporation, was demonstrated to be adjustable, varying the concentration of the PDMS solution and the number of impregnation steps. The thermal diffusion of the nanopapers was correlated with both the density of the nanopapers and the GNP contents, leading to in-plane diffusivity values in the range between 10 and 50 mm^2/s. Depending on the nanopaper density and composition, the nanopapers' thermal conductivity (in-plane) was obtained in the range between 5 and 25 W/m·K, along with the modulus and resistance up to 52 and 0.45 MPa, respectively. In particular, PDMS cross-linking under pressure to densify the nanopapers was proven to enhance both the thermal conductivity and mechanical properties, with dramatic reinforcing compared with the unpressed nanopaper counterpart. Based on the results obtained, PDMS/GNP nanopapers appear to be a promising solution in a heat spreader application requiring flexibility and toughness, such as in modern flexible electronics, as well as in wearable and implantable devices.

Supplementary Materials: The following are available online at https://www.mdpi.com/article/10.3390/jcs5120309/s1, Figure S1: FESEM micrographs of GNP nanopaper impregnated with 9% 1× (**a**) 17% 1× (**b**) and 29% 1× (**c**) solution, Table S1: Density, porosity and thermal diffusivity values calculated for impregnated nanopapers, Figure S2: Thermal diffusivity of PDMS impregnated nanopapers, as a function of nanopaper density (**a**,**b**) and as a function of GNP content (**c**,**d**), Figure S3: Representative stress-strain curves from tensile tests.

Author Contributions: Conceptualization, A.F.; methodology, A.F. and D.B.; investigation, D.B. and E.F.; data curation, E.F. and D.B.; writing, review, and editing, D.B. and A.F.; supervision, A.F.; funding acquisition, A.F. All authors have read and agreed to the published version of the manuscript.

Funding: This work has received funding from the European Research Council (ERC) under the European Union's Horizon 2020 research and innovation programme grant agreement 639495—INTHERM—ERC-2014-STG.

Institutional Review Board Statement: Not applicable.

Informed Consent Statement: Not applicable.

Data Availability Statement: The full data related to results presented in this study are available on motivated request from the corresponding author.

Acknowledgments: Julio Gomez at Avanzare Innovación Tecnólogica (Spain) is gratefully acknowledged for providing GNP. Mauro Raimondo and Dario Pezzini at Politecnico di Torino are also acknowledged for SEM observations.

Conflicts of Interest: The authors declare no conflict of interest. The funders had no role in the design of the study; in the collection, analyses, or interpretation of data; in the writing of the manuscript; or in the decision to publish the results.

References

1. Gadipelli, S.; Guo, Z.X. Graphene-based materials: Synthesis and gas sorption, storage and separation. *Prog. Mater. Sci.* **2015**, *69*, 1–60. [CrossRef]
2. Novoselov, K.S.; Fal'ko, V.I.; Colombo, L.; Gellert, P.R.; Schwab, M.G.; Kim, K. A roadmap for graphene. *Nature* **2012**, *490*, 192–200. [CrossRef] [PubMed]
3. Ferrari, A.C.; Bonaccorso, F.; Fal'ko, V.; Novoselov, K.S.; Roche, S.; Boggild, P.; Borini, S.; Koppens, F.H.; Palermo, V.; Pugno, N.; et al. Science and technology roadmap for graphene, related two-dimensional crystals, and hybrid systems. *Nanoscale* **2015**, *7*, 4598–4810. [CrossRef]
4. Backes, C.; Abdelkader, A.M.; Alonso, C.; Andrieux-Ledier, A.; Arenal, R.; Azpeitia, J.; Balakrishnan, N.; Banszerus, L.; Barjon, J.; Bartali, R.; et al. Production and processing of graphene and related materials. *2D Mater.* **2020**, *7*, 022001. [CrossRef]
5. Colonna, S.; Battegazzore, D.; Eleuteri, M.; Arrigo, R.; Fina, A. Properties of Graphene-Related Materials Controlling the Thermal Conductivity of Their Polymer Nanocomposites. *Nanomaterials* **2020**, *10*, 2167. [CrossRef] [PubMed]
6. Burger, N.; Laachachi, A.; Mortazavi, B.; Ferriol, M.; Lutz, M.; Toniazzo, V.; Ruch, D. Alignments and network of graphite fillers to improve thermal conductivity of epoxy-based composites. *Int. J. Heat Mass Transf.* **2015**, *89*, 505–513. [CrossRef]
7. Burger, N.; Laachachi, A.; Ferriol, M.; Lutz, M.; Toniazzo, V.; Ruch, D. Review of thermal conductivity in composites: Mechanisms, parameters and theory. *Prog. Polym. Sci.* **2016**, *61*, 1–28. [CrossRef]
8. Chen, H.; Ginzburg, V.V.; Yang, J.; Yang, Y.; Liu, W.; Huang, Y.; Du, L.; Chen, B. Thermal conductivity of polymer-based composites: Fundamentals and applications. *Prog. Polym. Sci.* **2016**, *59*, 41–85. [CrossRef]
9. Di Pierro, A.; Mortazavi, B.; Fina, A. Molecular Junctions Enhancing Thermal Transport within Graphene Polymer Nanocomposite: A Molecular Dynamics Study. *Nanomaterials* **2021**, *11*, 2480. [CrossRef]
10. Wang, Y.; Zhan, H.F.; Xiang, Y.; Yang, C.; Wang, C.M.; Zhang, Y.Y. Effect of Covalent Functionalization on Thermal Transport across Graphene–Polymer Interfaces. *J. Phys. Chem. C* **2015**, *119*, 12731–12738. [CrossRef]
11. Balandin, A.A. Thermal properties of graphene and nanostructured carbon materials. *Nat. Mater.* **2011**, *10*, 569–581. [CrossRef] [PubMed]
12. Tortello, M.; Colonna, S.; Bernal, M.; Gomez, J.; Pavese, M.; Novara, C.; Giorgis, F.; Maggio, M.; Guerra, G.; Saracco, G.; et al. Effect of thermal annealing on the heat transfer properties of reduced graphite oxide flakes: A nanoscale characterization via scanning thermal microscopy. *Carbon* **2016**, *109*, 390–401. [CrossRef]
13. Colonna, S.; Monticelli, O.; Gomez, J.; Novara, C.; Saracco, G.; Fina, A. Effect of morphology and defectiveness of graphene-related materials on the electrical and thermal conductivity of their polymer nanocomposites. *Polymer* **2016**, *102*, 292–300. [CrossRef]
14. Sheshkar, N.; Verma, G.; Pandey, C.; Sharma, A.K.; Gupta, A. Enhanced thermal and mechanical properties of hydrophobic graphite-embedded polydimethylsiloxane composite. *J. Polym. Res.* **2021**, *28*, 403. [CrossRef]
15. Kong, K.T.S.; Mariatti, M.; Rashid, A.A.; Busfield, J.J.C. Enhanced conductivity behavior of polydimethylsiloxane (PDMS) hybrid composites containing exfoliated graphite nanoplatelets and carbon nanotubes. *Compos. Part B Eng.* **2014**, *58*, 457–462. [CrossRef]
16. Zhao, Y.-H.; Zhang, Y.-F.; Bai, S.-L. High thermal conductivity of flexible polymer composites due to synergistic effect of multilayer graphene flakes and graphene foam. *Compos. Part A Appl. Sci. Manuf.* **2016**, *85*, 148–155. [CrossRef]
17. Zhang, Q.; Xu, X.; Li, H.; Xiong, G.; Hu, H.; Fisher, T.S. Mechanically robust honeycomb graphene aerogel multifunctional polymer composites. *Carbon* **2015**, *93*, 659–670. [CrossRef]
18. Tao, Z.; Wang, H.; Li, X.; Liu, Z.; Guo, Q. Expanded graphite/polydimethylsiloxane composites with high thermal conductivity. *J. Appl. Polym. Sci.* **2017**, *134*, 44843. [CrossRef]
19. Oliva, J.; Mtz-Enriquez, A.; Oliva, A.; Ochoa-Valiente, R.; Garcia, C.; Pei, Q. Flexible graphene composites with high thermal conductivity as efficient heat sinks in high-power LEDs. *J. Phys. D Appl. Phys.* **2018**, *52*, 025103. [CrossRef]
20. Han, B.; Song, J.; Hu, T.; Ye, H.; Xu, L. High thermal conductivity in polydimethylsiloxane composite with vertically oriented graphene nanosheets by liquid-phase exfoliation. *Chem. Phys. Lett.* **2020**, *743*, 137156. [CrossRef]
21. Fang, H.; Zhao, Y.; Zhang, Y.; Ren, Y.; Bai, S.-L. Three-dimensional graphene foam-filled elastomer composites with high thermal and mechanical properties. *ACS Appl. Mater. Interfaces* **2017**, *9*, 26447–26459. [CrossRef]

22. Zhao, Y.-H.; Wu, Z.-K.; Bai, S.-L. Study on thermal properties of graphene foam/graphene sheets filled polymer composites. *Compos. Part A Appl. Sci. Manuf.* **2015**, *72*, 200–206. [CrossRef]
23. Renteria, J.D.; Ramirez, S.; Malekpour, H.; Alonso, B.; Centeno, A.; Zurutuza, A.; Cocemasov, A.I.; Nika, D.L.; Balandin, A.A. Strongly Anisotropic Thermal Conductivity of Free-Standing Reduced Graphene Oxide Films Annealed at High Temperature. *Adv. Funct. Mater.* **2015**, *25*, 4664–4672. [CrossRef]
24. Shen, B.; Zhai, W.; Zheng, W. Ultrathin Flexible Graphene Film: An Excellent Thermal Conducting Material with Efficient EMI Shielding. *Adv. Funct. Mater.* **2014**, *24*, 4542–4548. [CrossRef]
25. Xin, G.; Sun, H.; Hu, T.; Fard, H.R.; Sun, X.; Koratkar, N.; Borca-Tasciuc, T.; Lian, J. Large-Area Freestanding Graphene Paper for Superior Thermal Management. *Adv. Mater.* **2014**, *26*, 4521–4526. [CrossRef]
26. Bernal, M.M.; Tortello, M.; Colonna, S.; Saracco, G.; Fina, A. Thermally and Electrically Conductive Nanopapers from Reduced Graphene Oxide: Effect of Nanoflakes Thermal Annealing on the Film Structure and Properties. *Nanomaterials* **2017**, *7*, 428. [CrossRef] [PubMed]
27. Wu, H.; Drzal, L.T. Graphene Nanoplatelet Paper as a Light-weight Composite with Excellent Electrical and Thermal Conductivity and Good Gas Barrier Properties. *Carbon* **2012**, *50*, 1135–1145. [CrossRef]
28. Chen, H.; Müller, M.B.; Gilmore, K.J.; Wallace, G.G.; Li, D. Mechanically Strong, Electrically Conductive, and Biocompatible Graphene Paper. *Adv. Mater.* **2008**, *20*, 3557–3561. [CrossRef]
29. Huang, W.; Ouyang, X.; Lee, L.J. High-performance nanopapers based on benzenesulfonic functionalized graphenes. *ACS Nano* **2012**, *6*, 10178–10185. [CrossRef]
30. Korkut, S.; Roy-Mayhew, J.D.; Dabbs, D.M.; Milius, D.L.; Aksay, I.A. High surface area tapes produced with functionalized graphene. *ACS Nano* **2011**, *5*, 5214–5222. [CrossRef] [PubMed]
31. Ferraro, G.; Bernal, M.M.; Carniato, F.; Novara, C.; Tortello, M.; Ronchetti, S.; Giorgis, F.; Fina, A. Bispyrene Functionalization Drives Self-Assembly of Graphite Nanoplates into Highly Efficient Heat Spreader Foils. *ACS Appl. Mater. Interfaces* **2021**, *13*, 15509–15517. [CrossRef]
32. Zeng, X.; Ye, L.; Yu, S.; Li, H.; Sun, R.; Xu, J.; Wong, C.-P. Artificial nacre-like papers based on noncovalent functionalized boron nitride nanosheets with excellent mechanical and thermally conductive properties. *Nanoscale* **2015**, *7*, 6774–6781. [CrossRef] [PubMed]
33. Huang, C.; Cheng, Q. Learning from nacre: Constructing polymer nanocomposites. *Compos. Sci. Technol.* **2017**, *150*, 141–166. [CrossRef]
34. Zhang, Y.; Gong, S.; Zhang, Q.; Ming, P.; Wan, S.; Peng, J.; Jiang, L.; Cheng, Q. Graphene-based artificial nacre nanocomposites. *Chem. Soc. Rev.* **2016**, *45*, 2378–2395. [CrossRef]
35. Li, D.B.K.; Pérez-Camargo, R.A.; Liu, G.; Monticelli, O.; Müller, A.J.; Fina, A. Polycaprolactone adsorption and nucleation onto graphite nanoplates for highly flexible, thermally conductive and thermomechanically stiff nanopapers. *ACS Appl. Mater. Interfaces* **2021**. accepted.
36. Colonna, S.; Bernal, M.M.; Gavoci, G.; Gomez, J.; Novara, C.; Saracco, G.; Fina, A. Effect of Processing Conditions on the Thermal and Electrical Conductivity of Poly (butylene terephthalate) Nanocomposites Prepared via Ring-Opening Polymerization. *Mater. Des.* **2017**, *119*, 124–132. [CrossRef]
37. Bernal, M.M.; Di Pierro, A.; Novara, C.; Giorgis, F.; Mortazavi, B.; Saracco, G.; Fina, A. Edge-Grafted Molecular Junctions between Graphene Nanoplatelets: Applied Chemistry to Enhance Heat Transfer in Nanomaterials. *Adv. Funct. Mater.* **2018**, *28*, 1706954. [CrossRef]